Inorg. Chem. **2004**, *43*, 1723–1734

Excited-State Characters and Dynamics of $[W(CO)_5(4\text{-cyanopyridine})]$ and $[W(CO)_5(piperidine)]$ Studied by Picosecond Time-Resolved IR and Resonance Raman Spectroscopy and DFT Calculations: Roles of W → L and W → CO MLCT and LF Excited States Revised

Stanislav Záliš,*,† Michael Busby,‡ Tomáš Kotrba,†,§ Pavel Matousek,|| Mike Towrie, and Antonín Vlček, Jr.*,†,‡

J. Heyrovský Institute of Physical Chemistry, Academy of Sciences of the Czech Republic, Dolejškova 3, CZ-182 23 Prague, Czech Republic, Department of Chemistry and Centre for Materials Research, Queen Mary, University of London, Mile End Road, London E1 4NS, United Kingdom, Central Laser Facility, CCLRC Rutherford Appleton Laboratory, Chilton, Didcot, Oxfordshire OX11 0QX, United Kingdom, and Institute of Chemical Technology, Technická 5, 166 28 Prague, Czech Republic

Received September 15, 2003

The characters, dynamics, and relaxation pathways of low-lying excited states of the complexes $[W(CO)_5L]$ [L = 4-cyanopyridine (pyCN) and piperidine (pip)] were investigated using theoretical and spectroscopic methods. DFT calculations revealed the delocalized character of chemically and spectroscopicaly relevant molecular orbitals and the presence of a low-lying manifold of CO π^*-based unoccupied molecular orbitals. Traditional ligand-field arguments are not applicable. The lowest excited states of $[W(CO)_5(pyCN)]$ are W → pyCN MLCT in character. They are closely followed in energy by W → CO MLCT states. Excitation at 400 or 500 nm populates the ^{3}MLCT(pyCN) excited state, which was characterized by picosecond time-resolved IR and resonance Raman spectroscopy. Excited-state vibrations were assigned using DFT calculations. The ^{3}MLCT(pyCN) excited state is initially formed highly excited in low-frequency vibrations which cool with time constants between 1 and 20 ps, depending on the excitation wavelength, solvent, and particular high-frequency ν(CO) or ν(CN) mode. The lowest excited states of $[W(CO)_5(pip)]$ are W → CO MLCT, as revealed by TD-DFT interpretation of a nanosecond time-resolved IR spectrum that was measured earlier in a low-temperature glass (Johnson, F. P. A.; George, M. W.; Morrison, S. L.; Turner, J. J. *J. Chem. Soc., Chem. Commun.* **1995**, 391–393). MLCT(CO) excitation involves transfer of electron density from the W atom and, to a lesser extent, the trans CO to the π^* orbitals of the four cis CO ligands. Optical excitation into MLCT(CO) transition of either complex in fluid solution triggers femtosecond dissociation of a W–N bond, producing $[W(CO)_5(solvent)]$. It is initially vibrationally excited both in ν(CO) and anharmonicaly coupled low-frequency modes. Vibrational cooling occurs with time constants of 16–22 ps while the intramolecular vibrational energy redistribution from the $v = 1$ ν(CO) modes is much slower, 160–220 ps. No LF excited states have been found for the complexes studied in a spectroscopically relevant range up to 6–7 eV. It follows that spectroscopy, photophysics, and photochemistry of $[W(CO)_5L]$ and related complexes are well described by an interplay of close-lying MLCT(L) and MLCT(CO) excited states. The high-lying LF states play only an indirect photochemical role by modifying potential energy curves of MLCT(CO) states, making them dissociative.

Introduction

Group 6 metal pentacarbonyls $[M(CO)_5L]$ (M = Cr, Mo, W; L = pyridine derivatives R-py or amines) play an important role in the development of our understanding of organometallic spectroscopy, photophysics, and photochemistry.[1−12] Some of these complexes have been implicated[11,13] in photocatalysis, since highly reactive coordinatively unsaturated species can be generated upon irradiation. Absorption spectra of $[M(CO)_5L]$ complexes show several bands that were originally attributed to ligand field (LF) transitions from predominantly d_π to d_{σ^*} metal orbitals and to M → py MLCT transitions, further abbreviated MLCT(py). Complexes with L = amine were thought to show only LF transitions while electron-accepting R-pyridine ligands introduce the possibility of M → py MLCT excitation.[1] The

* To whom correspondence should be addressed. E-mail: a.vlcek@qmul.ac.uk (A.V.).
† Academy of Sciences of the Czech Republic.
‡ University of London.
§ Institute of Chemical Technology.
|| CCLRC Rutherford Appleton Laboratory.

(1) Wrighton, M. S.; Abrahamson, H. B.; Morse, D. L. *J. Am. Chem. Soc.* **1976**, *98*, 4105.

10.1021/ic035089z CCC: $27.50
Published on Web 02/10/2004

relative energies of MLCT(py) and alleged LF excited states in [M(CO)$_5$(R-py)] depend[1,3,4] on the substituent R whereby electron-withdrawing substituents, such as CN, C(O)CH$_3$, or halide, push the MLCT(py) states low in energy making them the lowest excited states. The MLCT(py) and presumed LF transitions can be distinguished in the absorption spectra by their solvatochromism: the position of the MLCT(py) transition shifts significantly to lower energies as the solvent polarity decreases whereas the bands attributed to LF transitions are independent of the solvent. In fact, they depend only little even on the metal and the ligand L, occurring at around 400 nm. The model based on the interplay between LF and MLCT(py) excited states was used also to explain photophysics and photochemistry of [M(CO)$_5$L] complexes. Thus, for example, [W(CO)$_5$(R-py)] complexes with the lowest MLCT(py) excited states show long-lived (~300 ns) double emission in fluid solution that was attributed to two ^{3}MLCT(py) excited states.[3,5] Indeed, ^{3}MLCT(py) states were directly characterized by nanosecond time-resolved IR spectroscopy for R = CN and C(O)CH$_3$.[7,8] Photochemical substitution of the R-py ligand in these complexes is rather inefficient under irradiation into the MLCT(py) absorption band in the visible spectral region.[1,3,4] It occurs by a thermally activated population of higher states of an alleged LF character from a ^{3}MLCT(py) state.[2−4,7,8,12] The photochemical quantum yield increases on moving the irradiation wavelength into the near-UV region. On the other hand, complexes in which MLCT(py) states lie above the presumed LF states or amine complexes with no MLCT(L) states are highly photoreactive, losing the ligand L upon irradiation into their lowest absorption band.[1,14,15] [W(CO)$_5$(pip)] (pip = piperidine) in a low-temperature glass shows emission that was originally attributed to a LF state.[1] The nanosecond time-resolved IR spectrum of this excited state shows ν(CO) bands downshifted from their respective ground-state values.[9] This observation was explained by an admixture of CO π^* orbitals into the d-based LUMO.[9]

The LF/MLCT model originates in a traditional view of bonding in carbonyl complexes, whereby the d orbitals are split to d_π and d_{σ^*} sets while essentially maintaining their identity in the resulting molecular orbitals. Electron-accepting, reducible organic ligands insert their π^* orbitals between the two d-based sets, while CO π^* orbitals are assumed to lie at much higher energies. This simple approach is usually taken for granted, being used in textbooks and review articles without questioning. However, recent theoretical and experimental results have pointed to some essential flaws involved: (i) DFT[16−18] and CASSCF/CASPT2[19] calculations on M(CO)$_6$ (M = Cr, Mo, W) and Ni(CO)$_4$ have shown that LF excited states lie at much higher energies than was previously assumed. The lowest-lying excited states have been calculated as M → CO MLCT, further abbreviated as MLCT(CO). Nevertheless, extension of this conclusion to mixed-ligand carbonyl complexes is not straightforward since substitution of one or more CO ligands by a "weaker-field" N-donor is generally assumed to diminish the energy-splitting between predominantly metal-d unoccupied molecular orbitals and, hence, the LF excited-state energies. (ii) Our CASSCF/CASPT2 calculations[20,21] of [Cr(CO)$_4$(bpy)] and TD-DFT calculations[22−24] of [W(CO)$_4$(phen)], [W(CO)$_4$(tmp)], [W(CO)$_4$(^{i}Pr-DAB)], and, especially,[24] [W(CO)$_4$(en)] have found LF-like states only at very high energies. The lowest MLCT(diimine) excited states are immediately followed in energy by several MLCT(CO) states, while all the absorption bands of [W(CO)$_4$(en)] correspond to MLCT(CO) transitions. Moreover, the molecular orbitals involved are highly delocalized. The 5d(W) character was found to be distributed over many more molecular orbitals than predicted by the traditional ligand-field approach, while neither of them contains a predominant 5d(W) component. (iii) TD-DFT calculations[23] of triplet excited states of [W(CO)$_4$(phen)] and [W(CO)$_4$(tmp)] have attributed the high-energy emission to ^{3}MLCT(CO) excited states instead of ^{3}LF states, since the latter were calculated to lie at far too high energies. Similarly, emission from [W(CO)$_4$(en)] originates in an ^{3}MLCT(CO) excited state, which was also characterized experimentally by picosecond TRIR spectroscopy.[24] (iv) A TD-DFT theoretical study[25] of [Cr(CO)$_5$(PH$_3$)] has identified its lowest excited state as MLCT(CO), followed in energy by a mixed 50% MLCT(CO)/50% LF state. (v) Low-lying MLCT(CO) excited states were also identified computationally[26] for CpM(CO)$_2$ (M = Rh, Ir) complexes, which are important in photochemical activation of C−H bonds.[27−29]

(2) Lees, A. J.; Adamson, A. W. *J. Am. Chem. Soc.* **1980**, *102*, 6874.
(3) Lees, A. J.; Adamson, A. W. *J. Am. Chem. Soc.* **1982**, *104*, 3804.
(4) Kolodziej, R. M.; Lees, A. J. *Organometallics* **1986**, *5*, 450.
(5) Rawlins, K. A.; Lees, A. J.; Adamson, A. W. *Inorg. Chem.* **1990**, *29*, 3866.
(6) Wieland, S.; van Eldik, R.; Crane, D. R.; Ford, P. C. *Inorg. Chem.* **1989**, *28*, 3663.
(7) Glyn, P.; Johnson, F. P. A.; George, M. W.; Lees, A. J.; Turner, J. J. *Inorg. Chem.* **1991**, *30*, 3543.
(8) Johnson, F. P. A.; George, M. W.; Turner, J. J. *Inorg. Chem.* **1993**, *32*, 4226.
(9) Johnson, F. P. A.; George, M. W.; Morrison, S. L.; Turner, J. J. *J. Chem. Soc., Chem. Commun.* **1995**, 391.
(10) Lees, A. J. *Chem. Rev.* **1987**, *87*, 711.
(11) Geoffroy, G. L.; Wrighton, M. S. *Organometallic Photochemistry*; Academic Press: New York, 1979.
(12) Vlček, A., Jr. *Coord. Chem. Rev.* **1998**, *177*, 219.
(13) Wrighton, M. S.; Ginley, D. S.; Schroeder, M. A.; Morse, D. L. *Pure Appl. Chem.* **1975**, *41*, 671.
(14) Moralejo, C.; Langford, C. H. *Inorg. Chem.* **1991**, *30*, 567.
(15) Moralejo, C.; Langford, C. H.; Sharma, D. K. *Inorg. Chem.* **1989**, *28*, 2205.
(16) Pollak, C.; Rosa, A.; Baerends, E. J. *J. Am. Chem. Soc.* **1997**, *119*, 7324.
(17) Rosa, A.; Baerends, E. J.; van Gisbergen, S. J. A.; van Lenthe, E.; Groeneveld, J. A.; Snijders, J. G. *J. Am. Chem. Soc.* **1999**, *121*, 10356.
(18) Baerends, E. J.; Rosa, A. *Coord. Chem. Rev.* **1998**, *177*, 97.
(19) Pierloot, K.; Tsokos, E.; Vanquickenborne, L. G. *J. Phys. Chem.* **1996**, *100*, 16545.
(20) Guillaumont, D.; Daniel, C.; Vlček, A., Jr. *Inorg. Chem.* **1997**, *36*, 1684.
(21) Guillaumont, D.; Daniel, C.; Vlček, A., Jr. *J. Phys. Chem. A* **2001**, *105*, 1107.
(22) Farrell, I. R.; Hartl, F.; Záliš, S.; Mahabiersing, T.; Vlček, A., Jr. *J. Chem. Soc., Dalton Trans.* **2000**, 4323.
(23) Farrell, I. R.; van Slageren, J.; Záliš, S.; Vlček, A., Jr. *Inorg. Chim. Acta* **2001**, *315*, 44.
(24) Záliš, S.; Farrell, I. R.; Vlček, A., Jr. *J. Am. Chem. Soc.* **2003**, *125*, 4580.
(25) Goumans, T. P. M.; Ehlers, A. W.; van Hemert, M. C.; Rosa, A.; Baerends, E. J.; Lammertsma, K. *J. Am. Chem. Soc.* **2003**, *125*, 3558.
(26) Hu, Z.; Boyd, R. J.; Nakatsuji, H. *J. Am. Chem. Soc.* **2002**, *124*, 2664.
(27) Dunwoody, N.; Lees, A. J. *Organometallics* **1997**, *16*, 5770.

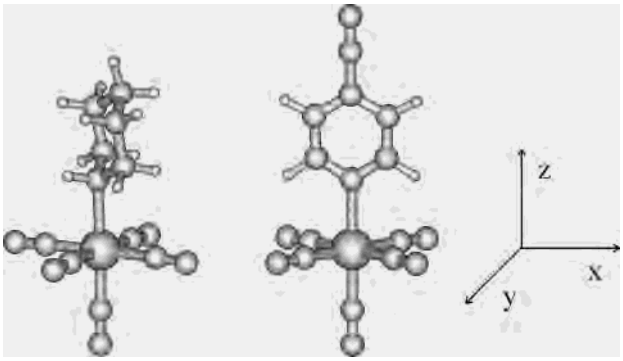

Figure 1. Schematic molecular structures of the complexes [W(CO)$_5$(pip)] (left) and [W(CO)$_5$(pyCN)] in the 45° conformation (right) and chosen orientation of axes. (In the 0° conformation, the py ligand plane (*xz*) contains also one of the cis OC−W−CO linkages.)

All these new theoretical and experimental results suggest that MLCT(CO) excited states play a very important role in the spectroscopy and photochemistry of mixed-ligand carbonyl complexes, while the importance and occurrence of LF states is questionable. A general conclusion emerges that the traditional MLCT(L)/LF model should be replaced by a new MLCT(L)/(CO) model in which the absorption and emission are determined by low-lying MLCT(L) and MLCT(CO) excited states.

Herein, we report results of our combined theoretical (TD-DFT) and spectroscopic investigations of the character and ultrafast dynamics of low-lying excited states of [W(CO)$_5$(pyCN)] and [W(CO)$_5$(pip)] complexes (pyCN = 4-cyanopyridine, pip = piperidine), Figure 1. It is argued that the MLCT(L)/(CO) model accounts well for the spectroscopic, photophysical, and photochemical properties of these mixed-ligand carbonyl complexes.

Experimental Section

Materials. [W(CO)$_5$(pyCN)] and [W(CO)$_5$(pip)] complexes were synthesized using literature methods[1] and purified by column chromatography. All spectroscopic measurements were carried out in spectroscopically pure CH_3CN or methylcyclohexane (MCH), both purchased from Aldrich.

Spectroscopic Techniques. The time-resolved visible, IR, Kerr-gate resonance Raman, and Kerr-gate emission instrumentation and procedures used were described in detail previously.[30−36] In short, the sample solution was excited (pumped) at 400 nm, using frequency-doubled pulses from a Ti:sapphire laser of ∼200 fs duration (fwhm) in the case of time-resolved visible and IR absorption spectroscopy, while pulses of 1−2 ps duration were used for Raman and emission studies. Optical parametric amplifiers were used to generate visible pump pulses in the 490−520 nm range. TRIR spectra were probed with IR (∼200 fs) pulses obtained by difference-frequency generation. The IR probe pulses cover a spectral range 150−200 cm^{-1} wide. Kerr-gate TR^3 spectra were measured using 1−2 ps, 400 nm pump pulses and probed at 400 nm using an OPA or frequency-doubled Ti:sapphire laser pulses, respectively. The Kerr gate was opened for ca. 4 ps coincidentally with the arrival of Raman photons and then closed to suppress all the long-lived emission from the Raman signal. TR^3 spectra were corrected for the Raman signal due to the solvent and the ground state by subtracting the spectra obtained at negative time delays (−50 and −20 ps) and by subtracting any weak residual emission that passes through the Kerr gate in the closed state. A ground-state (pre)resonance Raman spectrum of [W(CO)$_5$(pyCN)] was obtained using the Kerr-gate TR^3 instrument with the pump-beam blocked. The ground-state Raman scattering is then generated by the probe beam while the interfering emission is again removed by the Kerr gate. Spectral intensities were not corrected for spectrometer transmission.

All Raman spectra were measured from sample solutions flowed as a 0.5 mm diameter open jet. A 0.5 mm flow-through rastering CaF_2 cell was used to obtain TRIR spectra. The pump and infrared probe beams are focused to an area of less than 200 μm diameter.

Quantum Chemical Calculations. The ground-state electronic structures of [W(CO)$_5$(py)], [W(CO)$_5$(pyCN)], and [W(CO)$_5$(pip)] complexes were calculated by density functional theory (DFT) methods using the ADF2000.03[37,38] and Gaussian 98[39] program packages. The low-lying excited states of the closed-shell complexes were calculated by the time-dependent DFT (TD-DFT, both ADF and G98 programs). ADF, Gaussian 98, and Gaussian 03 were used for the calculations of the vibrational frequencies which were performed at optimized geometries corresponding to the functional and basis set used. The excited-state IR spectra were modeled by unrestricted Kohn−Sham calculations for the lowest lying triplet states described by their predominant single-determinant wave function revealed by TD-DFT. Changes in electron-density distribution upon excitation were calculated as difference electron densities between the ground state and the investigated excited state, as described by TD-DFT(G98). The difference density plots were prepared using the GaussView software.

Within Gaussian 98, Dunning's polarized valence double-ζ basis sets[40] were used for H, C, N, and O atoms and the quasirelativistic effective core pseudopotentials and corresponding optimized set

(28) Lees, A. J. *J. Organomet. Chem.* **1998**, *554*, 1.
(29) Bromberg, S. E.; Yang, H.; Asplund, M. C.; Lian, T.; McNamara, B. K.; Kotz, K. T.; Yeston, J. S.; Wilkens, M.; Frei, H.; Bergman, R. G.; Harris, C. B. *Science* **1997**, *278*, 260.
(30) Liard, D. J.; Busby, M.; Farrell, I. R.; Matousek, P.; Towrie, M.; Vlček, A., Jr. *J. Phys. Chem. A* **2004**, *108*, 556.
(31) Vlček, A., Jr.; Farrell, I. R.; Liard, D. J.; Matousek, P.; Towrie, M.; Parker, A. W.; Grills, D. C.; George, M. W. *J. Chem. Soc., Dalton Trans.* **2002**, 701.
(32) Matousek, P.; Parker, A. W.; Taday, P. F.; Toner, W. T.; Towrie, M. *Opt. Commun.* **1996**, *127*, 307.
(33) Towrie, M.; Parker, A. W.; Shaikh, W.; Matousek, P. *Meas. Sci. Technol.* **1998**, *9*, 816.
(34) Matousek, P.; Towrie, M.; Stanley, A.; Parker, A. W. *Appl. Spectrosc.* **1999**, *53*, 1485.
(35) Matousek, P.; Towrie, M.; Ma, C.; Kwok, W. M.; Phillips, D.; Toner, W. T.; Parker, A. W. *J. Raman Spectroc.* **2001**, *53*, 1485.
(36) Towrie, M.; Grills, D. C.; Dyer, J.; Weinstein, J. A.; Matousek, P.; Barton, R.; Bailey, P. D.; Subramaniam, N.; Kwok, W. M.; Ma, C. S.; Phillips, D.; Parker, A. W.; George, M. W. *Appl. Spectrosc.* **2003**, *57*, 367.
(37) Fonseca Guerra, C.; Snijders, J. G.; te Velde, G.; Baerends, E. J. *Theor. Chim. Acta* **1998**, *99*, 391.
(38) van Gisbergen, S. J. A.; Snijders, J. G.; Baerends, E. J. *Comput. Phys. Commun.* **1999**, *118*, 119.
(39) Frisch, M. J.; Trucks, G. W.; Schlegel, H. B.; Scuseria, G. E.; Robb, M. A.; Cheeseman, J. R.; Zakrzewski, V. G.; Montgomery, J. A., Jr.; Stratmann, R. E.; Burant, J. C.; Dapprich, S.; Millam, J. M.; Daniels, A. D.; Kudin, K. N.; Strain, M. C.; Farkas, O.; Tomasi, J.; Barone, V.; Cossi, M.; Cammi, R.; Mennucci, B.; Pomelli, C.; Adamo, C.; Clifford, S.; Ochterski, J.; Petersson, G. A.; Ayala, P. Y.; Cui, Q.; Morokuma, K.; Malick, D. K.; Rabuck, A. D.; Raghavachari, K.; Foresman, J. B.; Cioslowski, J.; Ortiz, J. V.; Baboul, A. G.; Stefanov, B. B.; Liu, G.; Liashenko, A.; Piskorz, P.; Komaromi, I.; Gomperts, R.; Martin, R. L.; Fox, D. J.; Keith, T.; Al-Laham, M. A.; Peng, C. Y.; Nanayakkara, A.; Gonzalez, C.; Challacombe, M.; Gill, P. M. W.; Johnson, B.; Chen, W.; Wong, M. W.; Andres, J. L.; Gonzalez, C.; Head-Gordon, M.; Replogle, E. S.; Pople, J. A. *Gaussian 98*, revision A.7; Gaussian. Inc.: Pittsburgh, PA, 1998.

of basis functions[41] for W. In these calculations, the hybrid Becke's three-parameter functional with the Lee, Yang, and Parr correlation functional (B3LYP)[42] was used (G98/B3LYP).

The ADF program used a local density approximation (LDA) with VWN parametrization of electron gas data and functional including Becke's gradient correction[43] to the local exchange expression in conjunction with Perdew's gradient correction[44] to the LDA expression (ADF/BP). The scalar relativistic (SR) zero order regular approximation[45] (ZORA) was used within ADF calculations. Slater-type orbital (STO) basis sets of triple-ζ quality with polarization functions were employed. The inner shells were represented by a frozen core approximation; viz., 1s for C, N, and O and 1s−4d for W were kept frozen. Compositions and energies of molecular orbitals and electronic transition energies and compositions were calculated by the asymptotically correct SAOP functional,[46] which is suitable also for higher-lying MO's and electronic transitions. Core electrons were included in ADF/SAOP calculations.

Geometry optimizations were carried out without any symmetry restriction. The approximate C_{2v} symmetry was used for the description of the spectra and molecular orbitals of py and pyCN complexes. Here, the *z*-axis is coincident with the C_2 symmetry axis, that is, with the N−W−CO link. The py or pyCN ligands are located in the *xz* plane, Figure 1. Structural optimization, vibrational analysis, and TD-DFT calculations of electronic transitions were performed for the 0 and 45° conformations (see Figure 1) of the complexes with planar ligands py and pyCN.

Results and Discussion

Molecular Structures. $[W(CO)_5(py)]$ and $[W(CO)_5(pyCN)]$ can exist in two conformations where the plane of the axial ligand either bisects the angle between the cis W−CO bonds or coincides with one of the cis OC−W−CO linkages; see Figure 1. Hereinafter, these conformations will be called 45 and 0°, respectively. Their total energies were calculated to be nearly identical in a vacuum, being separated by only a very low barrier (~35 cm^{-1}). Hence, $[W(CO)_5(py)]$ and $[W(CO)_5(pyCN)]$ are expected to exist in fluid solutions as an equilibrium mixture of both conformations.

Selected calculated bond lengths and angles of $[W(CO)_5(py)]$ and $[W(CO)_5(pyCN)]$ and $[W(CO)_5(pip)]$ are summarized in the Supporting Information. ADF/BP-calculated structures of $[W(CO)_5(py)]$ and $[W(CO)_5(pip)]$ agree very well with the experimental[47−49] ones, while G98/B3LYP slightly overestimates W−N and W−C bond lengths.

Vibrational Analysis of Electronic Ground State. Assuming a C_{4v} local symmetry, $[W(CO)_5L]$ complexes are expected[50,51] to show three IR-active ν(CO) vibrations, $2A_1$ + E. IR spectra are dominated by a strong E band. A weak A_1^2 band, which is predominantly due to an in-phase stretching vibration of the four cis CO ligands, occurs at higher frequencies. The A_1^1 ν(CO) vibration, which involves mainly the trans CO ligand, manifests itself by a shoulder on the low-energy side of the E band. Tables 1 and 2 compare the experimental and calculated ν(CO) wavenumbers of $[W(CO)_5(pyCN)]$ and $[W(CO)_5(pip)]$, respectively. The agreement is reasonable, although DFT calculations somewhat underestimate the wavenumber of the higher A_1^2 vibration while the E and A_1^1 wavenumbers are overestimated. In the actual C_{2v} symmetry of $[W(CO)_5(py)]$ and $[W(CO)_5(pyCN)]$, the E-mode is split into two closely spaced modes $B_1^2 + B_2$, both of which are IR-active. This splitting is larger in the 0° than 45° conformation where the four CO ligands are still equivalent. For example, E-band splitting of 11 and 1 cm^{-1} was calculated for 0 and 45° $[W(CO)_5(py)]$ in a vacuum. The predicted conformational effects on IR spectra are generally small and would be difficult to distinguish experimentally. In fact, only a single E band is seen in the solution or glass spectra of the complexes investigated herein.[7−9,52]

G98 DFT calculations were also used to assign the resonance Raman spectrum of $[W(CO)_5(pyCN)]$, Figure 2, bottom. The experimentally observed bands and their DFT-based assignments are summarized in Table 1.

Molecular Orbitals. Calculated energies and compositions of Kohn−Sham molecular orbitals of $[W(CO)_5(pip)]$ and $[W(CO)_5(pyCN)]$ in the 45° conformation are collected in Tables 3 and 4, respectively, while the Supporting Information summarizes MO's calculated for the 0° conformation

Table 1. Assignment of IR and Resonance Raman Spectra of the Ground and the a^3A_1 Lowest Triplet Excited States of $[W(CO)_5(pyCN)]$ (45°) Based on DFT G98/B3LYP-Calculated Frequencies with ν Indicating Stretching and δ In-Plane Bending Vibration Modes

ground state ν/cm^{-1}		excited state ν/cm^{-1}		
calcd[a]	expt	calcd[a]	expt	assgnt
403		344		ν(WC)
411		364		ν(WC)
435		379		$\nu(WC_{ax})$
485	478[b,c]	395		ν(WN) + $\nu(WC_{ax})$
767		732	760[e]	ν(WN) + δ(py ring)
989		985	975[e]	δ(py ring)
1047	1020[b]	1030		δ(py ring)
1184		1223		δ(C-H)
1222	1201[b]	1257	~1247[e]	δ(C-H)
1594	1612[b]	1593	1613[e]	ν(CC-py)
1947	1928[d]	1966	1964[f]	ν(CO), A_1^1
1949	1936[d]	1993	2002[f]	ν(CO), E
1950		1995		ν(CO), E
1980		1999		ν(CO), B_1
2058	2072[d]	2079	2146[f]	ν(CO), A_1^2
2261		2120	2105[f]	ν(CN) in MCH
2261	2247[b]	2120	2123[e]	ν(CN)

[a] Wavenumbers scaled by factor 0.961 recommended for calculation with double-ζ basis sets.[53] [b] rR in CH_2Cl_2. Very similar Raman wavenumbers were obtained in CH_3CN where the A_1^2 ν(CO) and the ν(CC-py) bands occur at 2082 and 1609 cm^{-1}, respectively. [c] Very weak Raman band. [d] FTIR in methylcyclohexane. [e] TR^3 in CH_3CN. [f] TRIR in methylcyclohexane.

(40) Woon, D. E.; Dunning, T. H., Jr. *J. Chem. Phys.* **1993**, *98*, 1358.
(41) Andrae, D.; Häussermann, U.; Dolg, M.; Stoll, H.; Preuss, H. *Theor. Chim. Acta* **1990**, *77*, 123.
(42) Stephens, P. J.; Devlin, F. J.; Cabalowski, C. F.; Frisch, M. J. *J. Phys. Chem.* **1994**, *98*, 11623.
(43) Becke, A. D. *Phys. Rev. A* **1988**, *38*, 3098.
(44) Perdew, J. P. *Phys. Rev. A* **1986**, *33*, 8822.
(45) van Lenthe, E.; Ehlers, A.; Baerends, E. J. *J. Chem. Phys.* **1999**, *110*, 8943.
(46) Schipper, P. R. T.; Gritsenko, O. V.; van Gisbergen, S. J. A.; Baerends, E. J. *J. Chem. Phys.* **2000**, *112*, 1344.
(47) Tutt, L.; Zink, J. I. *J. Am. Chem. Soc.* **1986**, *108*, 5830.
(48) Moralejo, C.; Langford, C. H.; Bird, P. H. *Can. J. Chem.* **1991**, *69*, 2033.
(49) Klement, U. *Z. Kristallogr.* **1993**, *208*, 111.
(50) Cotton, F. A. *Inorg. Chem.* **1964**, *3*, 702.
(51) Cotton, F. A.; Kraihanzel, C. S. *J. Am. Chem. Soc.* **1962**, *84*, 4432.
(52) Kraihanzel, C. S.; Cotton, F. A. *Inorg. Chem.* **1963**, *2*, 533.

Table 2. Comparison of G98/B3LYP-Calculated and Experimental CO Stretching Frequencies of the Ground and a^3A' Lowest Triplet Excited States of [W(CO)$_5$(pip)]

ground state ν/cm^{-1}				a^3A excited state ν/cm^{-1}			
G03/B3LYP calcd[a]	ADF/BP calcd	expt soln	expt glass	G03/B3LYP calcd[a]	ADF/BP calcd	expt glass	assgnt
1937	1936	1916	1898	1927	1874	1855	A_1[1]
1940	1938	1927	1920	1941	1879	1788	E
1940	1948	1927	1920	1954	1902	1788	E
1971	1969			1961	1933	1942	B_1
2057	2050	2070	2069	2045	2013		A_1[2]

[a] Ground-state experimental data are from isooctane solution[1] and 77 K methylcyclohexane glass.[9] Excited-state experimental spectrum was measured by nanosecond time-resolved IR spectroscopy in a 77 K methylcyclohexane glass.[9] G98-calculated wavenumbers are scaled by factor 0.961 recommended for calculation with double-ζ basis sets.[53]

Table 3. DFT ADF/SAOP-Calculated One-Electron Energies and Compositions of Selected Highest Occupied and Low-Lying Unoccupied Molecular Orbitals of [W(CO)$_5$(pip)] Expressed in Terms of Composing Fragments[a]

MO	*E*/eV	prevailing character	W	$(CO)_{cis}$	$(CO)_{trans}$	pip
			Unoccupied MO's			
70a′	−2.59	W + pip + CO	28 (s); 17 (d_σ)	11	16	25
43a″	−2.70	W + pip + CO	57 (d_σ)	18		25
66a′	−3.51	CO + pip + W	27 (d_π)	43		30
41a″	−3.78	CO + pip + W	31 (d_π)	44	12	12
65a′	−3.80	CO + pip + W	25 (d_π)	37	8	27
64a′	−4.31	pip + W	15 (s); 5 (d_σ)	8	4	68
40a″	−4.89	π CO		35	63	
39a″	−4.92	π CO		34	64	
63a′	−5.03	π CO		94	2	
38a″	−6.00	π CO		96		
37a″	−6.29	π CO		97	1	
62a′	−6.33	π CO	3 (p_x)	94	2	
61a′	−6.87	π CO	7 (p_y); 3 (d_π)	86		3
			Occupied MO's			
60a′	−9.60	$d_W + \pi$ CO	61 (d_π)	28	12	
36a″	−9.62	$d_W + \pi$ CO	60 (d_π)	27	13	
59a′	−10.02	$d_W + \pi$ CO	56 (d_π)	43		
58a′	−11.59	pip	4 (p_y)	4		90

[a] Calculated using a C_2 symmetry.

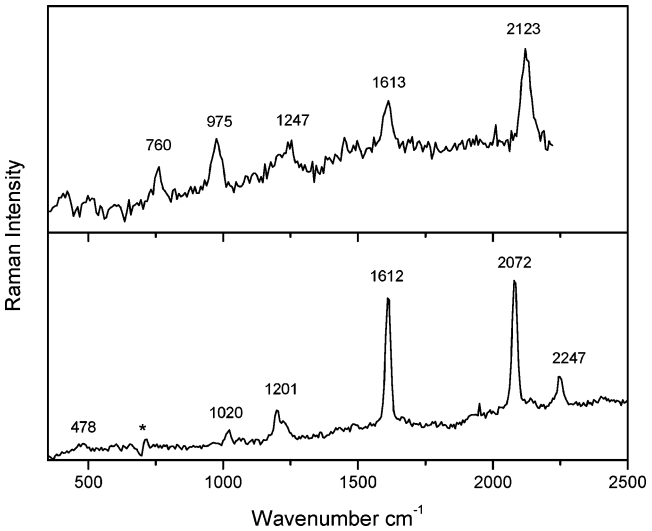

Figure 2. Ground- and excited-state resonance Raman spectra of [W(CO)$_5$(pyCN)]. Bottom: Ground-state resonance Raman spectrum of [W(CO)$_5$(pyCN)] measured in CH_2Cl_2 using 1−2 ps probe pulses at 400 nm and ~4 ps Kerr gate to remove emission. Top: Excited-state resonance Raman spectrum measured using 400 nm, 1−2 ps probe at 100 ps after 400 nm, 1−2 ps excitation in CH_3CN. The asterisk indicates a solvent band.

of [W(CO)$_5$(pyCN)] and for both conformations of [W(CO)$_5$(py)]. MO energies and compositions calculated for the py and pyCN complexes are almost independent of the conformation chosen, 45 or 0°.

The three highest occupied MOs are very similar in character for all three complexes investigated. They are almost 60% d_π in character. The cis and trans CO π* orbitals contribute approximately 25 and 15%, respectively, through the W → CO π* back-donation. The LUMO of [W(CO)$_5$(py)] and [W(CO)$_5$(pyCN)] is predominantly (96%) π* py or pyCN in character. It is followed in energy by a manifold of four unoccupied MOs that are predominantly composed of cis CO π* orbitals. For [W(CO)$_5$(pip)], the lowest member of this manifold, 61a′, is the LUMO. An analogous orbital is the LUMO + 1 in [W(CO)$_5$(py)] or LUMO + 2 in [W(CO)$_5$(pyCN)]. MOs with significant trans CO π* contributions occur at higher energies, above cis π* CO-based orbitals. Three closely spaced delocalized d_π/π*(CO) molecular orbitals that are π-antibonding with respect to W−C bonds lie still higher. The $d_{\sigma*}$-type orbitals occur at very high energies and are largely delocalized. For [W(CO)$_5$(pyCN)], the lowest MO with a significant (57%) $d_{\sigma*}$ contribution lies 7.17 eV above the HOMO. The MO pattern calculated herein for [W(CO)$_5$L] complexes does not conform to the usual textbook picture of ligand-field and simple MO theories. All molecular orbitals containing d-orbitals are highly delocalized, at least six molecular orbitals contain significant d_π contributions, and several $d_{\sigma*}$-based orbitals lie at very high energies, being highly mixed in character.

Table 4. DFT ADF/SAOP-Calculated One-Electron Energies and Compositions of Selected Highest Occupied and Low-Lying Unoccupied Molecular Orbitals of $[W(CO)_5(pyCN)]$ (45° Conformation) Expressed in Terms of Composing Fragments

MO	*E*/eV	prevailing character	W	$(CO)_{cis}$	$(CO)_{trans}$	pyCN
			Unoccupied MO's			
$49a_1$	−2.71	d_W	3 (s); 46 (d_{z^2})	7	18	25
$15a_2$	−2.79	d_W + CO	57 (d_{xy})	40		
$46a_1$	−3.86	π CO + d_W	40 ($d_{x^2-y^2}$)	56	1	
$25b_1$	−3.95	π CO + d_W	34 (d_{xz})	38	20	6
$29b_2$	−4.28	π CO + d_W	36 (d_{yz})	52	3	7
$45a_1$	−4.33	pyCN	17 (s); 2 (d_{z^2}); 2 ($d_{x^2-y^2}$)	2	2	74
$24b_1$	−5.00	π pyCN		17	5	75
$23b_1$	−5.09	π CO		34	63	3
$28b_2$	−5.09	π CO	5 (d_{yz})	15	78	2
$14a_2$	−5.16	π CO		98		
$27b_2$	−5.48	π pyCN			2	97
$13a_2$	−6.25	π CO		98		
$22b_1$	−6.55	π CO	3 (p_x)	95		
$26b_2$	−6.60	π CO	3 (p_y)	93	2	
$44a_1$	−7.04	π CO	8 (p_z); 3 (d_{z^2})	84		2
$12a_2$	−7.18	π pyCN		8		92
$21b_1$	−8.27	π pyCN	1 (d_{xz})		3	96
			Occupied MO's			
$20b_1$	−9.96	d_W + π CO	52 (d_{xz})	24	15	7
$25b_2$	−10.00	d_W + π CO	57 (d_{yz})	27	15	
$43a_1$	−10.35	d_W + π CO	57 ($d_{x^2-y^2}$)	43		
$11a_2$	−12.38	pyCN		1		98

Table 5. Selected TD-DFT-Calculated Low-Lying Singlet Excitation Energies (eV) for $[W(CO)_5(pip)]$ with Oscillator Strength Larger than 0.001[a]

		ADF/SAOP		G98/B3LYP			
state	composn (ADF/SAOP)	transition/eV (nm)	osc str	transition/eV (nm)	osc str	expt	ext coeff
b^1A'	86% (60a′ → 61a′), 8% (36a″ → 38a″), 5% (59a′ → 62a′)	2.91 (426)	0.010	3.01 (411)	0.013	407	3960
a^1A''	86% (36a″ → 61a′), 7% (60a′ → 38a″), 6% (59a′ → 37a″)	2.92 (424)	0.010	3.02 (410)	0.014		
d^1A'	56% (60a′ → 62a′), 43% (36a″ → 37a″)	3.29 (377)	0.004	3.63 (342)	0.010	380	sh
j^1A'	68% (60a′ → 64a′), 12% (58a′ → 62a′)	5.23 (237)	0.061	5.27 (235)	0.081	243	~38 000
j^1A''	63% (36a″ → 64a′), 18% (58a′ → 37a″)	5.25 (236)	0.055	5.29 (234)	0.103		

[a] Experimental spectra were measured in isooctane. Data are from ref 1. Extinction coefficients are in M^{-1} cm^{-1}.

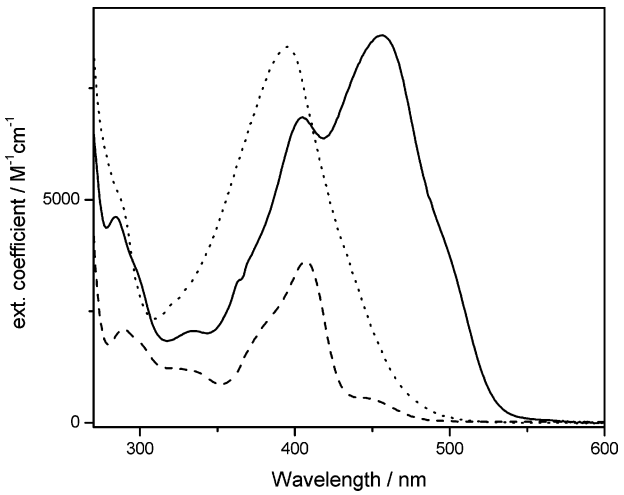

Figure 3. Electronic absorption spectra of $[W(CO)_5(pyCN)]$ in methylcyclohexane (MCH) (solid), $[W(CO)_5(pyCN)]$ in CH_3CN (dotted), and $[W(CO)_5(pip)]$ in MCH (dashed).

Electronic Transitions and Excited States. Absorption spectra of $[W(CO)_5(pip)]$ and $[W(CO)_5(pyCN)]$ are shown in Figure 3, while Tables 5 and 6 compare the experimental and calculated transition energies. The lowest allowed transition of $[W(CO)_5(pyCN)]$ is assigned as MLCT(pyCN). It is closely followed in energy by a manifold of low-lying MLCT(CO) transitions. The lowest allowed transition of $[W(CO)_5(pip)]$ is MLCT(CO) in character. For either complex, no LF transitions were found among the lowest 40 calculated transitions in a spectroscopically relevant range up to 6−7 eV.

In particular, the lowest two transitions of $[W(CO)_5(pip)]$ were identified as $a^1A' \rightarrow b^1A'$ and $a^1A \rightarrow a^1A''$ which are both MLCT(CO). Their principal (86%) components involve excitation from the HOMO set into the 61a′ LUMO, that is mainly cis CO π^*, Tables 3 and 5. The two other main contributing excitations are directed into 38a″, 62a′, or 37a″ orbitals, which all have cis π^* CO contributions larger than 90% (Table 3). The detailed character of the $a^1A' \rightarrow b^1A'$ transition is revealed by the calculated changes of electron density distribution shown in Figure 4. An extensive $W \rightarrow CO_{cis}$ charge transfer is accompanied by a small shift of electron density from the trans to cis CO ligands and a very small increase of electron density on the pip ligand.

The $a^1A \rightarrow b^1A', a^1A''$ MLCT(CO) transitions are responsible for the absorption band that was observed at 407 nm, Figure 3 and Table 5. The relatively large intensity of this band (ϵ = 3960 M^{-1} cm^{-1}) supports the MLCT(CO) character, as opposed to the traditional LF assignment. The MLCT(CO) character is also supported by the preresonance Raman spectrum,[47] which shows a strong enhancement of ν(CO) bands, of several low-wavenumber bands at 414, 426, and 433 cm^{-1}, which are assigned herein by DFT calculations as ν(WC), and of a band at 484 cm^{-1}, which originates in a

Table 6. Selected TD-DFT-Calculated Low-Lying Singlet Excitation Energies of [W(CO)$_5$(pyCN)] (45°)[a]

		ADF/SAOP		G98/B3LYP			
state	composn (ADF/SAOP)	transition/eV (nm)	osc str	transition/eV (nm)	osc str	expt	ext coeff
a^1A_2	79% ($25b_2 \rightarrow 21b_1$)	1.75 (708)		2.25 (551)			
b^1B_1	98% ($43a_1 \rightarrow 22b_1$)	2.08 (596)	0.001	2.59 (478)	0.001		
b^1A_1	98% ($20b_1 \rightarrow 21b_1$)	2.09 (593)	0.213	2.43 (509)	0.191	454[b]	8680[c]
c^1B_1	81% ($20b_1 \rightarrow 44a_1$), 8% ($25b_2 \rightarrow 13a_2$) 8% ($43a_1 \rightarrow 22b_1$)	3.13 (396)	0.010	3.07 (404)	0.012	399[b]	7280[c]
b^1B_2	79% ($25b_2 \rightarrow 44a_1$), 9% ($20b_1 \rightarrow 13a_2$)	3.04 (408)	0.009	3.10 (399)	0.009	355	
g^1B_2	78% ($43a_1 \rightarrow 28b_2$), 12% ($43a_1 \rightarrow 26b_2$)	5.20 (238)	0.094	5.30 (234)	0.095	243	~60800
g^1B_1	71% ($43a_1 \rightarrow 23b_1$), 13% ($43a_1 \rightarrow 22b_1$)	5.21 (238)	0.097	5.33 (233)	0.075		
h^1A_1	65% ($19b_1 \rightarrow 21b_1$), 19% ($20b_1 \rightarrow 24b_1$)	5.31 (233)	0.216	5.54 (223)	0.141		

[a] Experimental spectra were measured in methylcyclohexane. Extinction coefficients are in M^{-1} cm^{-1} [b] Obtained by Gaussian fitting of the spectrum. [c] Data are from ref 3.

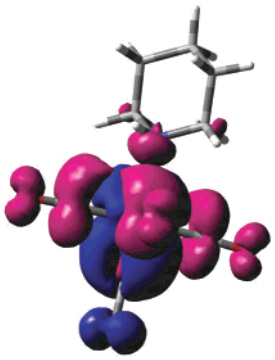

Figure 4. Change of electron density distribution upon the $a^1A' \rightarrow b^1A'$ electronic transition of [W(CO)$_5$(pip)]. Blue and violet colors correspond to a decrease and increase of electron density, respectively. Values were calculated from G98/B3LYP TD-DFT densities.

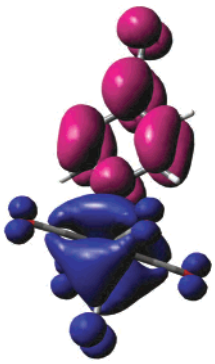

Figure 5. Change of electron density distribution upon the $a^1A_1 \rightarrow b^1A_1$ electronic transition of [W(CO)$_5$(pyCN)]. Blue and violet colors correspond to a decrease and increase of electron density, respectively. Values were calculated from G98/B3LYP TD-DFT densities.

highly mixed deformation vibration with ν(WC) and ν(WN) contributions. Notably, the 2069 cm^{-1} A_1^2 band, which corresponds predominantly to cis ν(CO), shows a strong enhancement, in agreement with the expected large shift of electron density to cis CO.

The low-energy band observed at 443 nm ($\epsilon = 560$ M^{-1} cm^{-1}) is attributed to spin-forbidden MLCT(CO) transitions into a^3A' and a^3A'' states, which originate in ~98% HOMO $\rightarrow$ LUMO and HOMO $-$ 1 $\rightarrow$ LUMO excitations, respectively. They were both calculated at ~2.55 eV, that is, 494 nm. Accordingly, emission of [W(CO)$_5$(pip)], observed[5] in low-temperature glasses at 532 nm ($\tau = 4.7$ μs) is attributed herein to the radiative decay of these two ^{3}MLCT(CO) states. The MLCT(CO) character of the lowest triplet state of [W(CO)$_5$(pip)] is further supported by its TRIR spectra; vide infra.

In the case of [W(CO)$_5$(pyCN)], the electron-accepting pyCN ligand introduces a π*(pyCN) LUMO (Table 4) and, hence, low-lying MLCT(pyCN) excited states, Table 6. Accordingly, the lowest allowed electronic transition was identified as $a^1A_1 \rightarrow b^1A_1$ MLCT(pyCN). It originates in nearly pure (98%) HOMO $\rightarrow$ LUMO excitation. The MLCT(pyCN) character is further confirmed by the calculated electron density changes, Figure 5, which show that the electron density is transferred from the whole W(CO)$_5$ fragment to the pyCN ligand, including the CN group.

The $a^1A_1 \rightarrow b^1A_1$ MLCT(pyCN) transition gives rise to the intense solvatochromic band (Figure 3) observed at 454 nm in MCH (395 nm in CH_3CN). The low-energy shoulder at 505 nm (455 nm in CH_3CN) is assigned either to a symmetry-forbidden $a^1A_1 \rightarrow a^1A_2$ transition calculated at 2.25 eV (551 nm) or to a spin-forbiden ^{3}MLCT(pyCN) transition. The latter assignment is supported by the absence of any low-energy shoulders in the spectra of Mo pentacarbonyls, including [Mo(CO)$_5$(pyCN)].[4]

The MLCT(pyCN) transitions are closely followed in energy by two MLCT(CO) transitions to c^1B_1 and b^1B_2 states, whose principal contributing excitations involve excitation into predominantly cis CO π* orbitals. These two transitions are essentially identical in character with the lowest two transitions of [W(CO)$_5$(pip)]. The $a^1A_1 \rightarrow c^1B_1$,$b^1B_2$ MLCT(CO) transitions are responsible for the strong absorption band at 400 nm (in MCH) and the shoulder at 370 nm, Table 6.

The assignment of the lowest allowed transition of [W(CO)$_5$(pyCN)] as MLCT(pyCN) is confirmed by the resonance Raman spectrum (Figure 2, bottom, and Table 1), which shows a typical MLCT pattern.[54,55] The strong enhancement of the A_1^2 ν(CO) band stems from changes in C$\equiv$O bonding due to a decrease of electron density on the W(CO)$_5$ fragment upon MLCT excitation. Resonance enhancement from the nearby MLCT(CO) transitions may also contribute. Apparent reduction of the pyCN ligand in the MLCT excited state is manifested by the strong enhancement of the intra-pyridine ν(CC), δ(CH), and δ(py-ring) and, especially, of the ν(CN) vibrations. The latter indicates the

(53) Wong, M. W. *Chem. Phys. Lett.* **1996**, *256*, 391.
(54) Stufkens, D. J. *Coord. Chem. Rev.* **1990**, *104*, 39.
(55) Vlček, A. J. *Coord. Chem. Rev.* **2002**, *230*, 225.

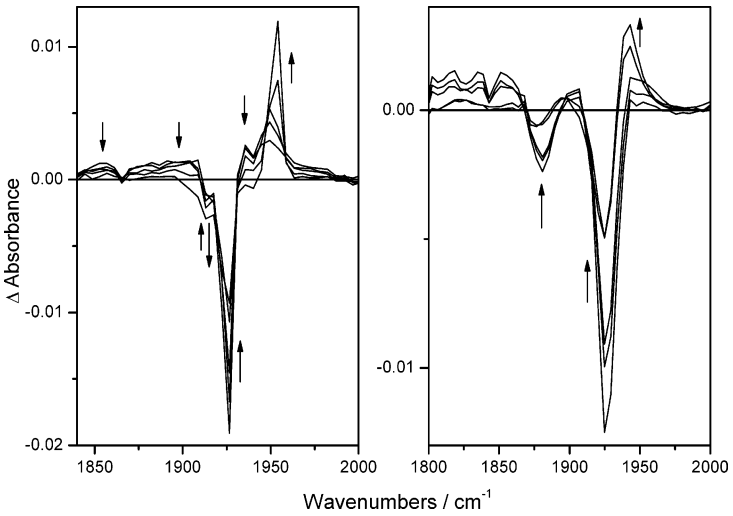

Figure 6. Picosecond time-resolved spectra of $[W(CO)_5(pip)]$ measured at 2, 3, 7, 40, and 1000 ps after ~200 fs, 400 nm excitation: left, methylcyclohexane (MCH) solution; right, CH_3CN solution. The spectra evolve in the direction of arrows.

important role of the CN group in accepting the excited electron density, in accordance with the calculated changes of the electron-density distribution, Figure 5.

TD-DFT calculations predict that electronic transitions of the two possible conformations of $[W(CO)_5(pyCN)]$ are essentially identical in energies, intensities, and characters. For example, the lowest allowed MLCT(pyCN) transition of the 45° conformation was calculated at 2.43 eV with the oscillator strength 0.199. The corresponding values for the 0° conformation are 2.50 eV and 0.209, respectively. The differences are even smaller for other low-lying transitions; see the Supporting Information.

$[W(CO)_5(pyCN)]$ exhibits dual emission in fluid solution at 545 and 613 nm that decays with a rather long lifetime (τ = 292 ns in MCH at 296 K).[5] Analysis of the temperature dependence of the relative emission intensities has shown[5] that the two emissions originate in two thermally equilibrated MLCT(pyCN) excited states which differ in energy by 990 cm^{-1}. This assignment is supported by a rigidochromic blue-shift of both emission maxima to 489 and 593 nm in a 77 K EPA glass, where the two emitting states are no longer in thermal equilibrium (τ = 11.4 and 20.1 μs, respectively).[5] Our TD-DFT calculation revealed the presence of three low-lying triplet MLCT(pyCN) states at 1.99 eV (a^3A_1), 2.19 eV (a^3A_2), and 2.57 eV (a^3B_1). They are essentially single-determinant excitations, originating in different members of the HOMO set; see the Supporting Information. The double emission is attributed to two of these states, possibly (on symmetry arguments) a^3A_2 and a^3B_1.

For $[W(CO)_5(py)]$, the lowest allowed MLCT(py) and MLCT(CO) excited states lie very close in energy. The lack of solvatochromism of the lowest absorption band and the high photochemical quantum yield indicate that the lowest excited state is MLCT(CO). Accordingly, G98 TD-DFT calculation predicts the following order of electronic transitions: 3.08 eV (a^1B_1, MLCT(CO)); 3.13 eV (b^1A_1, MLCT(py)); 3.18 eV (a^1B_2, MLCT(CO)). The ADF/SAOP calculation produced a different order of electronic transitions that does not agree with experiments: 2.70 eV (b^1A_1); 2.90 eV (a^1B_1); 3.04 eV (a^1B_2) (see the Supporting Information for details). It should be noted, however, that the actual order of the MLCT(py) and MLCT(CO) states will also depend on the medium.

$[W(CO)_5(pip)]$ Excited-State Character: DFT Interpretation of an Excited-State IR Spectrum. An IR spectrum of the lowest excited state of $[W(CO)_5(pip)]$ was measured earlier in a methylcyclohexane/isopentane (5/1) glass at 90 K using a nanosecond TRIR spectrometer.[9] Experimental and calculated wavenumbers are summarized in Table 2. In agreement with the experiment, the DFT calculation predicts all ν(CO) wavenumbers to be lower in the MLCT(CO) state than in the ground state. However, the experimental intensities suggest that the A_1^1 band occurs at a higher wavenumber than the E band. This unusual order of the A_1^1 and E modes was not reproduced computationally, presumably due to the very shallow character of the energy minimum of the a^3A' potentially energy surface, which is (nearly) unbound along the W−N coordinate in fluid solutions (see below). The a^3A' state is stabilized against dissociation by confinement in a rigid glass, which can modify the IR band intensities and/or positions relative to those expected for an isolated molecule. The band at 1942 cm^{-1}, originally attributed to the A_1^2 mode, is reassigned herein to the B_1 mode that is calculated at 1933 cm^{-1} with an IR intensity 130-times higher than in the ground state. (The original A_1^2 assignment seems unrealistic since it would require a −127 cm^{-1} downward shift from the ground-state value, contrary to the calculated shift of −38 cm^{-1}. The expected position of the A_1^2 band is out of the range studied experimentally.[9]) Although the agreement between the calculated and experimental IR spectra is not perfect, it well supports the assignment of the lowest triplet state of $[W(CO)_5(pip)]$ as MLCT(CO).

Ultrafast Photochemistry of $[W(CO)_5(pip)]$: Time-Resolved IR (TRIR) Spectroscopy. TRIR spectra measured in MCH (Figure 6, left) show absorption features and ensuing

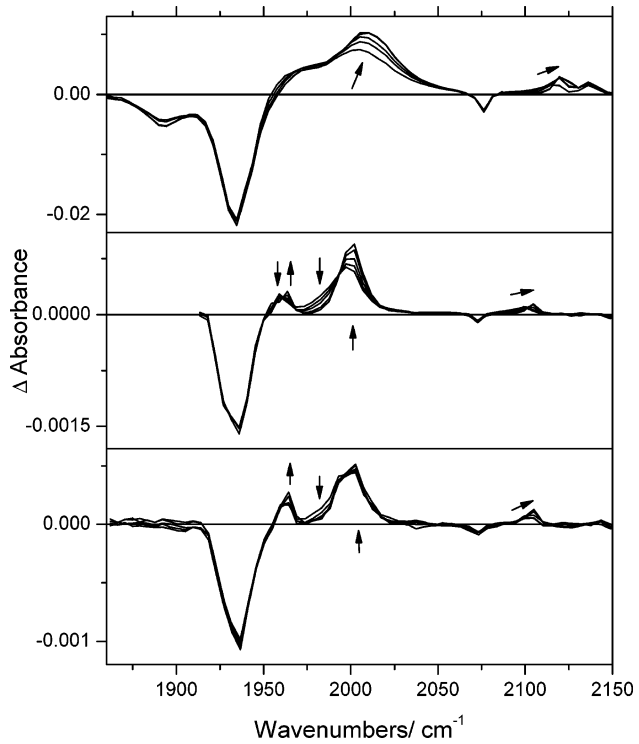

Figure 7. Picosecond time-resolved spectra of [W(CO)$_5$(pyCN)] measured at selected time delays after ~200 fs excitation. Experimental points are separated by ca. 4 cm^{-1}. The spectra evolve in the directions of the arrows. Top: CH_3CN solution excited at 400 nm. Time delays shown are 2, 4, 7, 40, and 200 ps. Middle: MCH solution excited at 400 nm. Time delays shown are 2, 4, 8, 20, and 300 ps. Bottom: MCH solution excited at 500 nm. Time delays shown are 2, 4, 8, 30, and 300 ps.

dynamics which are very similar to those observed[56,57] for [W(CO)$_5$(hexane)] produced by UV photolysis of W(CO)$_6$. Therefore, they are attributed to vibrational dynamics of the [W(CO)$_5$(MCH)] photoproduct. Optical excitation immediately produces negative bleach bands at 1913 and 1927 cm^{-1}, a broad, weak absorption that extends from ca. 1800 to at least 1909 cm^{-1}, where it overlaps with the bleach, and absorption bands at 1936 and ~1949 cm^{-1}. Using the arguments outlined previously,[56] we assign the 1900−1909 cm^{-1} feature, together with its low-wavenumber tail, and the 1936 cm^{-1} band to $v = 1 \rightarrow 2$ A_1^1 and E hot-bands of [W(CO)$_5$(MCH)], respectively. The 1949 cm^{-1} band corresponds to the $v = 0 \rightarrow 1$ E vibration of [W(CO)$_5$(MCH)], whose wavenumber is initially downshifted by anharmonic coupling with highly excited low-frequency modes. As the vibrational cooling proceeds, the 1949 cm^{-1} band shifts to 1954 cm^{-1}, which corresponds to the thermally equilibrated [W(CO)$_5$(MCH)] photoproduct.[7,8,56]

Kinetic analysis of the spectral evolution allows us to distinguish several processes which occur on different time scales: (i) ultrafast W−N(pip) bond dissociation that occurs in less than 1 ps, which is within the instrument time resolution and forms vibrationally highly excited [W(CO)$_5$(MCH)] photoproduct; (ii) initial vibrational cooling completed in 8−10 ps that is manifested by IR band narrowing and small upward shift; (iii) a ca. 20 ps vibrational cooling of low-frequency vibrations[57] which is manifested by a 20−22 ps component of the biexponential decay of the 1800−1909 and 1936 cm^{-1} bands and by a similar 15 ± 3 ps component of the biexponential rise of the 1954 cm^{-1} band; (iv) a 160−220 ps kinetic component was found for the decay of the 1900−1909 and 1936 cm^{-1} $v = 1 \rightarrow 2$ hot ν(CO) band and for the rise of the $v = 0 \rightarrow 1$ product band at 1954 cm^{-1}. It corresponds to vibrational relaxation of the $v = 1$ E and A_1^1 ν(CO) vibrational levels of the [W(CO)$_5$(MCH)] product. In agreement with this explanation, only the ~20 ps vibrational cooling, but not the slow kinetic component, was found at 1857 cm^{-1}, which is far away from the $v = 1 \rightarrow 2$ A_1^1 hot band.

The partial bleach recovery at 1927 cm^{-1} is single-exponential with a time constant of ca. 22 ps. It is attributed to the rise of overlapping positive photoproduct A_1^1 band expected[56] at 1928 cm^{-1}. At early time delays, this band occurs at lower wavenumbers and then narrows, increases in intensity, and moves across the bleach region with a ~20 ps time constant. This is manifested by the decrease of the 1927 cm^{-1} bleach and by the peculiar behavior of the 1913 cm^{-1} bleach, whose intensity sharply diminishes between 2 and 30 ps and then increases (becomes more negative) again until ca. 500 ps, when it is even more negative than at 2 ps. The deepening of the 1913 cm^{-1} bleach clearly excludes any possibility that some of the bleach dynamics can be caused by reformation of the parent [W(CO)$_5$(pip)].

Previous TRIR study of [W(CO)$_5$(hexane)] generated from W(CO)$_6$ has found[56] a weak $v = 1 \rightarrow 2$ A_1^1 transition at 1908 cm^{-1}, which is manifested in the spectra presented herein by the feature at 1900−1909 cm^{-1}. The hot $v = 1 \rightarrow 2$ E-band was found at 1942 cm^{-1}. Time constants of 22−26 and 160 ± 20 ps were determined[56,57] for the vibrational cooling and depopulation of the $v = 1$ ν(CO) levels, respectively. These values are very close to those measured in this study, where [W(CO)$_5$(MCH)] is photogenerated from [W(CO)$_5$(pip)].

TRIR spectra measured in acetonitrile (Figure 6, right) immediately (0−2 ps) after excitation show negative bands at 1880 and 1925 cm^{-1} due to the depleted ground-state population and a weak, very broad absorption that extends from ca. 1800 to at least 1910 cm^{-1}, where it overlaps with the bleach. Within the next ~40 ps the broad absorption decreases, both bleach bands diminish in intensity, and a new band at 1943 cm^{-1}, which corresponds[50] to [W(CO)$_5$(CH_3CN)], grows-in and concomitantly narrows. The time-constant values of all these processes are identical within the experimental uncertainty, 16 ps on the average. It is attributed to vibrational cooling of the [W(CO)$_5$(CH_3CN)] photoproduct. The decrease of the bleach bands amounts to ca. 20 and 40% of the initial absorbance at 1880 and 1925 cm^{-1}, respectively. (The apparent larger recovery of the 1925 cm^{-1} bleach is caused by its overlap with the growing A_1^1 product band[50] at 1931 cm^{-1}.) The $v = 1 \rightarrow 2$ hot bands were not observed in CH_3CN, perhaps due to much faster vibrational energy redistribution from $v = 1$ ν(CO) modes.

In conclusion, the ps TRIR spectra reported herein show that the MLCT(CO) excited state of [W(CO)$_5$(pip)] under-

(56) Dougherty, T. P.; Heilweil, E. J. *Chem. Phys. Lett.* **1994**, *227*, 19.
(57) Lian, T.; Bromberg, S. E.; Asplund, M. C.; Yang, H.; Harris, C. B. *J. Phys. Chem.* **1996**, *100*, 11994.

goes W−N bond dissociation producing [W(CO)$_5$(solvent)] in less than 1 ps. In methylcyclohexane, the [W(CO)$_5$(MCH)] photoproduct is formed highly vibrationally excited in low-frequency modes and also in ν(CO) A_1^1 and E modes, exactly in the same way as if produced from W(CO)$_6$. Finally, it should be noted that although the assignment[56] of the features at 1909 and 1936 cm^{-1} to the $v = 1 \rightarrow 2$ ν(CO) hot bands is convincing, alternative interpretations cannot be entirely excluded. For example, these two features can belong to electronically, instead of vibrationally, excited [W(CO)$_5$(MCH)] photoproduct.

Characterization of the Lowest Excited-State of [W(CO)$_5$(pyCN)] by Time-Resolved Resonance Raman (TR^3) Spectroscopy. The TR^3 spectrum (Figure 2, top, and Table 1) was measured using a probe wavelength of 510 nm which is close to a ∼520 nm maximum of a broad absorption of the MLCT(pyCN) excited state (see refs 3 and 58 and Figure 1 of the Supporting Information), which arises from a $\pi\pi^*$ transition of the reduced pyCN$^{\bullet-}$ ligand, present in the MLCT(pyCN) state. Accordingly, the TR^3 spectrum shows exclusively pyCN$^{\bullet-}$ vibrations. The ν(CN) band occurs at 2123 cm^{-1} in CH_3CN and at ∼2115 cm^{-1} in CH_2Cl_2, shifted upon excitation by ca. −130 cm^{-1} from the ground-state values. Such a large downward shift demonstrates that the pyCN ligand is virtually reduced in the MLCT(pyCN) state and that the extra electron density is largely localized at the CN group. The magnitude of this shift is comparable to that observed for intramolecular charge-transfer excited states in organic compounds such as 4-(dimethylamino)benzonitrile (−120 cm^{-1}).[59,60] The G98-DFT calculation of the a^3A_1 lowest MLCT(pyCN) excited state reproduces very well the ν(CN) wavenumber and its downward shift relative to the ground state, Table 1. The ν(CC) wavenumber is almost identical in the ground and excited state (∼1612 cm^{-1}), while the δ(CH) and δ(py) vibrations are shifted in the excited state by +54 and −45 cm^{-1}, respectively. Another pyCN$^{\bullet-}$ band was observed at 761 cm^{-1} and attributed by DFT to a coupled ν(WN)/δ(py) vibration. Overall, the excited-state TR^3 spectrum confirms the ^{3}MLCT character of the lowest excited state of [W(CO)$_5$(pyCN)] and shows that it can be formulated as [W$^{\text{I}}$(CO)$_5$(pyCN$^{\bullet-}$)]. Moreover, comparison of TR^3 spectra measured at different time delays shows that the ν(CN) band in acetonitrile initially occurs at ∼2108 cm^{-1} (extrapolated to $t = 0$) and shifts to its final position with a time constant of about 3.4 ps. This effect is due to cooling of initially highly excited low-frequency vibrational modes, which are anharmonically coupled to the ν(CN) mode. It follows that the ^{3}MLCT(pyCN) state is initially formed vibrationally hot.

Nature and Dynamics of Low-Lying Excited States of [W(CO)$_5$(pyCN)] Revealed by TRIR Spectroscopy. Picosecond TRIR spectra were measured after 400 or 500 nm excitation; see Figure 7. Spectra obtained at early time delays reveal rich vibrational dynamics that are more pronounced after 400 than 500 nm excitation; compare the middle and bottom panels in Figure 7. The spectral pattern measured at long time delays (≥20 ps) corresponds to the vibrationally relaxed MLCT(pyCN) excited state and does not depend on the excitation wavelength.

Excitation of [W(CO)$_5$(pyCN)] in methylcyclohexane at 500 nm is directed into the low-energy side of the b^1A_1 MLCT(pyCN) absorption band, Figure 3. The TRIR spectra (Figure 7, bottom) show negative (bleach) bands at 1937 and 2073 cm^{-1} due to the depleted ground-state population and positive bands at 1964, 2002, 2105, and 2146 cm^{-1}, which are assigned to the A_1^1 ν(CO), E ν(CO), ν(CN), and A_1^2 ν(CO) vibrations, respectively, of the a^3A_1 MLCT(pyCN) excited state, Table 1. This assignment is based on the similarity with the ground-state IR spectrum and relative band intensities. The ν(CN) band is identified by comparison with the TR^3 spectrum. The upward shift of the ν(CO) bands from their respective ground-state positions is fully supportive of a MLCT(pyCN) character of the photogenerated species. This is further confirmed by the comparison of the experimental spectral pattern with that calculated for the a^3A_1 MLCT(pyCN) excited state; see Table 1. The calculation correctly reproduces the upward shifts of ν(CO) wavenumbers and the downward shift of ν(CN), although the shift magnitudes are somewhat underestimated. Both the experimental and calculated spectra show a much larger difference between the E and A_1^1 wavenumbers in the ^{3}MLCT(pyCN) excited state than in the ground state, indicating structural changes of the W(CO)$_5$ fragment.

The intense and broad E band at 2002 cm^{-1} undergoes a dynamical narrowing and shift to higher wavenumbers by ca. +4 cm^{-1} with a time constant of 3.8 ± 0.7 ps. Very small shifts are seen also for the ν(CO) A_1^1 band (+0.7 cm^{-1}, 18 ± 7 ps) and the ν(CN) band (+0.8 cm^{-1}). This behavior is caused by relaxation (cooling) of anharmonically coupled low-frequency intramolecular, solute−solvent and first solvation shell vibrational modes, which are initially highly excited since they accept the energy released during the population of the ^{3}MLCT(py) state by intersystem crossing from the optically prepared ^{1}MLCT(py) Franck−Condon state.

Excitation at 400 nm of a MCH solution is directed into the MLCT(CO) absorption band maximum, Figure 3. Gaussian analysis of the UV−vis absorption spectrum revealed that the MLCT(CO) and MLCT(pyCN) transitions are optically excited in an approximate 2:1 ratio. TRIR spectra measured with 400 nm excitation show only bands due to the ^{3}MLCT(pyCN) and a very weak feature due to [W(CO)$_5$(MCH)]. It follows that the optically populated ^{1}MLCT(CO) state undergoes ultrafast internal conversion to ^{3}MLCT(pyCN) and a parallel low-yield W−N bond dissociation. The E band of the ^{3}MLCT(pyCN) state narrows by ∼40% and shifts upward by ∼4 cm^{-1} with time constants of 6.5 ± 0.6 and 6.0 ± 0.5 ps, respectively, Figure 8. The lowest A_1^1 ν(CO) mode exhibits more extensive dynamic changes than those observed after 500 nm excitation, Figures 7 and 8. The corresponding IR band undergoes a +2.3 cm^{-1} shift with a 19 ± 3 ps time constant that is accompanied by narrowing

(58) Lindsay, E.; Vlček, A., Jr.; Langford, C. H. *Inorg. Chem.* **1993**, *32*, 3822.
(59) Hashimoto, M.; Hamaguchi, H. *J. Phys. Chem.* **1995**, *99*, 7875.
(60) Kwok, W. M.; Ma, C.; George, M. W.; Grills, D. C.; Matousek, P.; Parker, A. W.; Phillips, D.; Toner, W. T.; Towrie, M. *Phys. Chem. Chem. Phys.* **2003**, *5*, 1043.

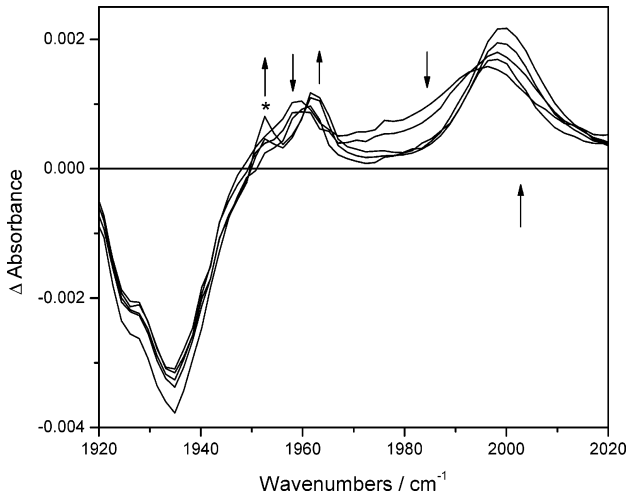

Figure 8. Details of the dynamical behavior of the A_1^1 and E bands of the MLCT(pyCN) excited state of $[W(CO)_5(pyCN)]$ measured in a MCH solution at 2, 5, 12, 60, and 500 ps after 400 nm, ~200 fs excitation. Experimental points are separated by ca. 2 cm^{-1}. The spectra evolve in the direction of arrows. An asterisk marks the $[W(CO)_5(MCH)]$ photoproduct band at 1953 cm^{-1}.

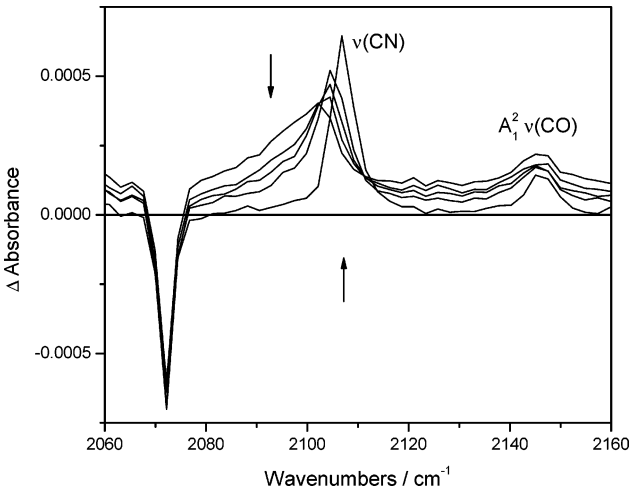

Figure 9. Details of the dynamical behavior of the ν(CN) and A_1^2 ν(CO) IR bands of the MLCT(pyCN) excited state of $[W(CO)_5(pyCN)]$ measured in a MCH solution at 2, 4, 6, 10, and 500 ps after 400 nm, ~200 fs excitation. Experimental points are separated by ca. 2 cm^{-1}. The spectra evolve in the direction of arrows.

and intensity increase. The dynamics of the A_1^2 ν(CO) and ν(CN) bands are shown in Figure 9. The highest A_1^2 ν(CO) band shows only a very small dynamic shift of about +1.8 cm^{-1} with an estimated time constant of 11 ps. The ν(CN) IR band shifts by +13 cm^{-1} with biexponential kinetics of 1.9 ± 0.3 and 15 ± 1 ps, which contribute approximately in a 2:1 ratio. Similarly, the ~3.9× narrowing of the ν(CN) band is biexponential with a dominating $\sim 1 \pm 0.2$ ps component and a much smaller 21 ± 7 ps contribution.

Close inspection of the high-wavenumber onset of the 1935 cm^{-1} bleach band (Figure 8) indicates the presence of a weak overlapping transient absorption at 1953 cm^{-1}, which is apparent from the early times after excitation (~3 ps) but grows in prominence with time. It is attributed[7] to the $[W(CO)_5(MCH)]$ photoproduct formed by an ultafast pyCN dissociation from the MLCT(CO) state. The apparent growth of this feature is due to vibrational cooling of $[W(CO)_5$-(MCH)]; vide supra. This 1953 cm^{-1} feature is absent in the spectra excited at 500 nm, in accord with the negligible photochemical quantum yield and a slow rate observed[1,3,7] under visible excitation, which populates the only the MLCT-(pyCN) state.

Excited-state behavior of $[W(CO)_5(pyCN)]$ in CH_3CN is very similar to that in MCH; see Figure 7, top. The ^{3}MLCT-(pyCN) E band occurs at ~2008 cm^{-1} and undergoes a small time-dependent upward shift and narrowing. The broad shoulder at about 1975 cm^{-1} encompasses the bands due to the A_1^1 vibration of the MLCT(pyCN) state and the $[W(CO)_5$-$(CH_3CN)]$ band expected[50] at 1948 cm^{-1}. The two weak bands in the high-wavenumber region at 2119 and 2135 cm^{-1} are attributed to the ν(CN) and A_1^2 ν(CO) vibrations, respectively, assigned by comparison with the DFT results (Table 1) and the TR[3] spectra (Figure 2).

Overall, TRIR spectra of $[W(CO)_5(pyCN)]$ show that 500 nm excitation populates the ^{3}MLCT(pyCN) excited state via intersystem crossing from the ^{1}MLCT(pyCN) state. Excitation at 400 nm populates the ^{3}MLCT(pyCN) state both through the ^{1}MLCT(pyCN) state and by an internal conversion/intersystem crossing from ^{1}MLCT(CO) state(s). In either case, the ^{3}MLCT(pyCN) state is initially formed vibrationally excited in low-frequency modes whose subsequent cooling is manifested by dynamical shifts of ν(CO) and ν(CN) bands, occurring with time constants in the range of 1−20 ps. This initial vibrational excitation seems to be more extensive following 400 than 500 nm excitation. Finally, it should be noted that neither of the TRIR spectra measured shows any evidence for the simultaneous presence of two excited species that is indicated by the double emission seen[5] in luminescence spectra. This can be explained by the low population of the higher-energy species (~25% can be estimated at 296 K for $\Delta E = 990$ cm^{-1})[5] and/or a close similarity of their IR spectra that is expected if both emitting species are MLCT-(pyCN) states. Moreover, no splitting of the E band, which would indicate a significant presence of the 0° conformation in the excited state, was observed.

Conclusions

Analysis of Kohn−Sham molecular orbitals calculated for $[W(CO)_5L]$ complexes (L = 4-cyanopyridine, pyridine, piperidine) reveals that the conventional ligand-field (LF) arguments are not applicable to interpret bonding, spectroscopy, photophysics, and photochemistry of heteroleptic pentacarbonyl complexes. Notably, all the MOs are largely delocalized, the d-character being distributed among more MOs than predicted by simple LF arguments. The character of the LUMO depends on L. Complexes where L is a strong π-acceptor (e.g. L = pyCN, py) have a predominantly π*-(L) LUMO that is closely followed in energy by a set of low-lying cis CO π* orbitals. Complexes where L is an electron-saturated ligand (pip) have a predominantly cis CO π*-based LUMO, followed by MOs of the same π*(CO) character. Orbitals with a significant d(σ*) contribution are also rather delocalized. They occur very high in energy, ≥7 eV above the HOMO.

Low-lying electronic transitions and excited states of

$[W(CO)_5L]$ and related complexes are of a W → L and W → CO MLCT character. No LF transitions were found to occur in a spectroscopically relevant energy range up to 6−7 eV. The lowest excited states have MLCT(CO) character for weakly electron-accepting or saturated ligands L (pip, py) and MLCT(L) character for strongly accepting L (pyCN). Spectroscopy, photophysics, and photochemistry of $[W(CO)_5L]$ and related complexes are described by the MLCT(L)/(CO) model in which the absorption, emission, and W−N bond dissociation are determined by closely lying MLCT(L) and MLCT(CO) excited states while the high-lying LF states play only an indirect photochemical role[16,18,25] by modifying potential energy curves of MLCT(CO) states, making them dissociative.

The lowest-lying ^{3}MLCT(pyCN) excited state of $[W(CO)_5(pyCN)]$ is initially formed excited in low-frequency vibrations that are anharmonically coupled to ν(CO) and ν(CN) modes. The dynamics of vibrational cooling depends on the particular high-frequency mode, excitation wavelength, and solvent. The corresponding time constants range from ∼1 to 20 ps. Conformational dynamics (rotation of the py plane relative to the $W(CO)_5$ unit) do not appear to have any important photophysical role.

The MLCT(CO) excited states of both $[W(CO)_5(pyCN)]$ and $[W(CO)_5(pip)]$ undergo femtosecond (<1 ps) dissociation of the W−N bond. The $[W(CO)_5(solvent)]$ photoproduct is formed vibrationally excited in high-frequency ν(CO) as well as in anharmonically coupled low-frequency modes. Vibrational cooling of the latter occurs with time constants of 16 and 22 ps in CH_3CN and methylcyclohexane, respectively, while the intramolecular redistribution of vibrational energy from the ν(CO) modes is much slower, 160−220 ps. Vibrational dynamics found herein for $[W(CO)_5(solvent)]$ produced from $[W(CO)_5(pip)]$ is essentially the same as that observed[56,57] when $[W(CO)_5(solvent)]$ had been photogenerated from $W(CO)_6$. This shows that the excess energy released by the W−N dissociation is in both cases transformed into the vibrational energy of the $W(CO)_5$ fragment, instead of being carried away in the form of a vibrational and/or translational energy of the dissociated pip or CO ligand. This observation agrees with the MLCT(CO) character of the reactive excited state in both cases, for which an extensive distortion of the $W(CO)_5$ fragment is expected.

$[W(CO)_5(pyCN)]$ is also known to undergo an inefficient "slow" (4 μs) photochemical dissociative substitution of the pyCN ligand upon irradiation in to the lowest ^{1}MLCT(pyCN) absorption band, which was shown to involve thermally activated population of an upper reactive excited state from the ^{3}MLCT(pyCN) state.[1,3,5−7] In view of the present results, this reactive state is assigned as MLCT(CO).

Acknowledgment. Dr. Mikhail Zimin of the Institute of Molecular Chemistry, University of Amsterdam, is thanked for measuring the time-resolved visible absorption spectrum. Funding from the EPSRC, Ministry of Education of the Czech Republic, and COST Action D14 is gratefully acknowledged.

Supporting Information Available: Additional tables and figure. This material is available free of charge via the Internet at http://pubs.acs.org.

IC035089Z